Copy No._____

Defence Research and   Recherche et développement
Development Canada   pour la défense Canada

DEFENCE **R&D** DÉFENSE

Modelling scattering from simple three-dimensional bathymetric features using wavefield superposition

J. Fawcett

Defence R&D Canada – Atlantic

Technical Memorandum
DRDC Atlantic TM 2006-086
August 2006

Canada

This page intentionally left blank.

Modelling scattering from simple three-dimensional bathymetric features using wavefield superposition

J. Fawcett

Defence Research & Development Canada Atlantic

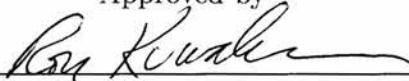Technical Memorandum

DRDC Atlantic TM 2006–086

August 2006

Author

John Fawcett

Approved by

Ron Kuwahara
Head/Signatures

Approved for release by

ᴅᴏⁿ Kirk Foster
Chair/Document Review Panel

Abstract

In this report we describe a method for modelling the scattering from three-dimensional bathymetric features on the seabed. In particular, the features are taken to be azimuthally symmetric about the z-axis. This approach could model seamount or basin type features or at higher frequencies, smaller protuberances and depressions. The method uses a set of point sources within the scattering region and exterior to the region to satisfy the appropriate continuity and boundary conditions along scattering features and seabed/water interface. Multi-frequency and Fourier-synthesized time domain responses for the scattering from such features are presented. In addition we present a semi-analytic modal solution which can be used as a benchmark for a bathymetric feature in a halfspace with only a change in density

Résumé

Dans le présent rapport, nous décrivons une méthode pour la modélisation de la diffusion à partir de caractéristiques bathymétriques tridimensionnelles du plancher océanique. Plus particulièrement, ces caractéristiques sont choisies de manière à ce qu'elles soient symétriques azimutalement par rapport à l'axe des "z". Cette méthode permet la modélisation de monts sous-marins ou de bassins ou, à des fréquences supérieures, de protubérances ou de dépressions. Cette méthode utilise un ensemble de sources ponctuelles situées à l'intérieur et à l'extérieur de la zone de diffusion afin de respecter les conditions adéquates de continuité et de limite le long de caractéristiques de diffusion et à l'interface plancher océanique-eau. Des réponses àdimension temporelle, multifréquences, par synthèse de Fourier, pour la diffusion par de telles caractéristiques éléments, sont présentées. Nous présentons également une solution modale semi-analytique qui peut être utilisée comme référence pour une caractéristique bathymétrique dans un demi-espace où il n'y a qu'une seule variation de densité.

Executive summary

BACKGROUND

The modelling and understanding of acoustic scattering from bathymetric features is important in a number of sonar applications where the scattering of acoustic energy from seabed features produces reverberation and highlight features which may interfere with the detection of objects of interest. These objects may be submarines or torpedoes within the water column or sea mines on the bottom or buried in the underlying sediment. Bathymetric features can also cast acoustic shadows affecting the detection of objects on the seabed and they can significantly alter the transmission of sonar energy into the sediment. This report presents a method for computing the acoustic scattering from simple three-dimensional bathymetric features on the seabed.

SIGNIFICANCE OF RESULTS

It is shown that the scattering from three-dimensional bathymetric features (with an azimuthal symmetry) can be modeled accurately and efficiently for low to moderate frequencies (e.g., a few kHz). The model allows one to accurately predict the effects of simple bathymetric features on the scattering and propagation of a sonar signal. The three-dimensional solutions which can be obtained from the methods of this report should prove useful as benchmark solutions for other scattering models.

FUTURE WORK

In the future, more general and efficient methods (although, perhaps more approximate) which could be used for more general seabed bathymetry and at higher frequencies than considered in this report, should be investigated. The methods described in this report could provide accurate and challenging benchmark cases.

Fawcett, J. Modelling scattering from simple three-dimensional bathymetric features using wavefield superposition. DRDC Atlantic TM 2006-086, Defence R&D Canada - Atlantic.

Sommaire

CONTEXTE

La modélisation et la compréhension de la diffusion acoustique à partir de caractéristiques bathymétriques sont importantes pour un grand nombre d'applications aux sonars, dans lesquelles la diffusion de l'énergie acoustique par des caractéristiques du plancher océanique produit de la réverbération et fait ressortir des caractéristiques qui peuvent interférer lors de la détection des objets recherchés. Ces objets peuvent être des sous-marins ou des torpilles se trouvant dans la colonne d'eau ou des mines marines déposées au fond ou enfouies dans les sédiments sous-jacents. Les caractéristiques bathymétriques peuvent également produire des ombres acoustiques qui influent sur la détection d'objets situés sur le plancher océanique et elles peuvent modifier considérablement la transmission de l'impulsion émise jusque dans les sédiments. Dans le présent rapport, on présente une méthode de traitement informatique de la diffusion acoustique produite par des caractéristiques bathymétriques tridimensionnelles simples du plancher océanique.

PORTÉE

Il est démontré que la diffusion par des caractéristiques bathymétriques tridimensionnelles (à symétrie azimutale) peut être modélisée avec précision et efficacement pour des fréquences de faibles à modérées (de quelques kHz). Le modèle permet de prédire avec précision les effets de caractéristiques bathymétriques simples sur la diffusion et la propagation du signal d'un sonar. Les solutions tridimensionnelles pouvant être obtenues par les méthodes figurant dans le présent rapport devraient être utiles comme solutions de référence pour d'autres modèles de diffusion.

RECHERCHES FUTURES

Dans l'avenir, des méthodes plus générales et efficaces (bien que, peut-être plus approximatives) pouvant être utilisées pour la bathymétrie plus générale et pour des fréquences plus élevées que celles considérées dans le présent rapport devraient être étudiées. Les méthodes décrites dans le présent rapport pourraient servir de références précises et rigoureuses.

Table of contents

List of figures

1 INTRODUCTION

The modelling of acoustic scattering from range-dependent bathymetry or surfaces is a subject of much interest in underwater acoustics. For example, bathymetric features can cause significant sonar returns, reverberation, which can interfere with the detection of a target (e.g., submarine, torpedo, mine). A bathymetric feature can cast an acoustic shadow on the seabed which may hinder the detection of mines located within this shadow. In addition, when searching for a buried target, the sonar signal which is transmitted into the underlying sediment may be significantly altered by the seabed features. At higher sonar frequencies, these effects can be caused by relatively small-sized features. Thus the ability to predict the effects of seabed bathymetry on sonar returns is important to understanding sonar system performance in a number of applications.

There have been many methods proposed for modelling propagation and scattering in three-dimensional, possibly range-dependent media. These include Parabolic Equation methods [1], coupled mode methods [2-4], boundary element methods [5], multipole expansion or wavefield superposition methods [6-8] and finite difference methods [9]. These various methods all have their advantages and disadvantages in terms of accuracy, computation efficiency and generality. In this report, we consider a scattering chamber/wavefield superposition method [10]. The scattering chamber refers to the fact that a small region surrounding the scattering feature of interest is defined and this region is coupled to the surrounding medium by a set of interior and exterior virtual sources. We will consider three-dimensional bathymetric features which are azimuthally-symmetric.

The advantages of the method of this report is that it reduces the computational domain to a region which encloses the scattering surface while still insuring that the resulting scattered fields satisfy the boundary conditions of the waveguide outside the scattering region. This type of approach was used in Ref.10 to model scattering from a rough sea surface. Wave superposition methods have also been used to model target scattering in a waveguide[7]. Schmidt[8] has combined the wave superposition method, Finite Element modelling and the OASES propagation code to obtain a computational method for partially-buried targets in a waveguide. Our approach for bathymetric scattering is conceptually similar to the target scattering case. We introduce an additional curve to make the bathymetric feature into a closed region which has the properties of one of the surrounding media. We represent the field interior to this region with a set of point sources (rather than using a finite element model) to characterize the region's interior fields and

we use another set of point sources in the interior of the region to represent the exterior field. These point sources in the interior are used in conjunction with the Green's Function for the surrounding medium, thus insuring that the appropriate boundary conditions (e.g., along the water/seabed interface) are satisfied. The point source coefficients are determined from a system of equations expressing the continuity conditions across the boundary defining the bathymetry region. Once the point source coefficients have been determined, the pressure field can be computed for an arbitrary receiver position. In addition, we will consider azimuthally-symmetric features. This allows us to solve the full three-dimensional scattering problem as a sequence of two-dimensional problems.

2 THEORY

For the pressure field, p, and the Green's Function G in an azimuthally symmetric waveguide we can write,

$$
\begin{aligned}
p(r, z, \theta) &= \sum_{m=0}^{\infty} p_m(r, z) \cos(m\theta) \\
p^{inc}(r, z, \theta) &= \sum_{m=0}^{\infty} p_m^{inc}(r, z) \cos(m\theta) \\
G(r, z, \theta; r', z', \theta') &= \sum_{m=0}^{\infty} g_m(r, z, ; r', z') \cos(m(\theta - \theta')),
\end{aligned}
\tag{1}
$$

where (r, z) is a two-dimensional cylindrical coordinate system and θ is the azimuthal angle about the axis of symmetry, the z-axis. The terms $g_m(r, z, ; r', z')$ are computed from the azimuthal transform of the Green's Function. In this report we will be considering both the Green's Function for three-dimensional free space and the Green's Function for a half space and their azimuthal transforms. For example, the half-space Green's Function for the mth azimuthal order can be written for the source point (r', z') in the upper half space,

$$
\begin{aligned}
g_m(r, z, ; r', z') &= \int_0^{\infty} J_m(pr) J_m(pr') \\
&\times \frac{(\exp(i\gamma_1 |z - z'|) + R(p) \exp(i\gamma_1(z + z')))}{i\gamma_1} p\,dp, z > 0 \\
&= \int_0^{\infty} J_m(pr) J_m(pr') \frac{T(p) \exp(-i(\gamma_2 z + \gamma_1 z'))}{i\gamma_1} p\,dp, z < 0
\end{aligned}
\tag{2}
$$

where $\gamma_1 \equiv \sqrt{\omega^2/c_1^2 - p^2}$ and $R(p)$ and $T(p)$ are the reflection and transmission coefficients for the incident field in the upper halfspace. A similar expression exists for the case that the source points are in the lower half space with $\gamma, R(p)$ and $T(p)$ replaced by the appropriate expressions.

The Green's Function in a free space is given by

$$
G(r, z, \theta; r', z', \theta') = \frac{\exp(i\omega R)}{R}
\tag{3}
$$

where

$$
R \equiv \sqrt{r^2 + r'^2 - 2rr' \cos(\theta - \theta') + (z - z')^2}.
\tag{4}
$$

[Many authors include a factor of 4π in the denominator of Eq.(3), but to simply our notation and to be consistent with Eq.(2), we will not include this factor]. The azimuthal transform of this function can be expressed as

$$g_m(r, z, ; r', z') = \int_0^\pi \frac{\exp(i\omega R)}{R} \cos(m\psi) d\psi \qquad (5)$$

where $\psi \equiv \theta - \theta'$, recalling from Eq.(4) that R depends on θ and θ' through their difference. There are a variety of analytical expressions for Eq.(5) either as a series of Legendre polynomials and spherical Hankel or Bessel functions or in terms of elliptical integrals [11]. Also, one can efficiently compute the expression for several values of m using FFT methods. The tradeoff, in this case, is the requirement to store the resulting values for subsequent computation. For this report, we simply discretize the integral of Eq.(5) and perform the integration numerically as required.

For the halfspace Green's Function, we can rewrite it in the form, for $z' \geq 0$

$$
\begin{aligned}
g_m(r, z, ; r', z') &= \int_0^\infty J_m(pr) J_m(pr') \\
&\times \frac{(R(p) - R_{as}) \exp(i\gamma_1(z + z')))}{i\gamma_1} p\,dp + t_{dir} + t_{ref}, z > 0 \\
&= \int_0^\infty J_m(pr) J_m(pr') \Big[\frac{T(p) \exp(-i(\gamma_2 z - \gamma_1 z'))}{i\gamma_1} \qquad (6) \\
&- \frac{T_{as} \exp(-i\gamma_2(z - z'))}{i\gamma_2} \Big] p\,dp \\
&+ t_{trans}, z < 0 \qquad (7)
\end{aligned}
$$

where

$$
\begin{aligned}
t_{dir} &= \int_0^\pi \frac{\exp(i\omega\sqrt{r^2 + r'^2 - 2rr'\cos\psi + (z - z')^2})}{\sqrt{r^2 + r'^2 - 2rr'\cos\psi + (z - z')^2}} \cos(m\psi) d\psi \\
t_{ref} &= R_{as} \int_0^\pi \frac{\exp(i\omega\sqrt{r^2 + r'^2 - 2rr'\cos\psi + (z + z')^2})}{\sqrt{r^2 + r'^2 - 2rr'\cos\psi) + (z + z')^2}} \cos(m\psi) d\psi \\
t_{trans} &= T_{as} \int_0^\pi \frac{\exp(i\omega_2\sqrt{r^2 + r'^2 - 2rr'\cos\psi + (z - z')^2})}{\sqrt{r^2 + r'^2 - 2rr'\cos\psi + (z - z')^2}} \cos(m\psi) d\psi \quad (8)
\end{aligned}
$$

$$(9)$$

and

$$
\begin{aligned}
R_{as} &= \frac{\rho_2 - \rho_1}{\rho_2 + \rho_1}, \\
T_{as} &= \frac{2\rho_2}{\rho_2 + \rho_1}. \qquad (10)
\end{aligned}
$$

The terms of Eq.(9) represent singular terms which occur for $z' \to z$, $r' \to r$ and for $z = 0$ (for t_{ref} and t_{trans}). In the case of a Boundary Integral Equation Method (BIEM), the singular behaviour of t_{dir}, t_{ref} and t_{trans} would need to be analytically accounted for. For the method of images considered in this paper, there will always be a non-zero distance between the source and the surface where the boundary conditions are applied. Similar expressions to those of Eqs.(9) and (10) are obtained for $z' < 0$. In Fig. 1 we show a schematic cross section of a "bump" on the seafloor. In this case the feature is pointing into the upper medium. The solid line is the actual bathymetry and the dashed line represents an arbitrary numerical boundary placed into the bottom. The squares represent sources placed a specified distance exterior to the region Ω and are used to represent the field within the region Ω. These are free space sources (suitable transformed into the azimuthal domain) with the sound speed c_2. The density within the regions is that of the lower halfspace ρ_2. The triangles represent sources shifted slightly to the interior of the bounding curve C and are associated with the half-space Green's Functions (in the azimuthally-transformed domain) for these particular source positions. The resultant exterior field satisfies the boundary conditions along the water/seabed interface. In the case that we are considering a basin (i.e., a negative deformation of the seabed) the situation is almost exactly the same, except that now the interior values for the sound speed and density for Ω are those of the upper half space. If a deformation is both positive and negative with respect to the flat surface $z = 0$m, then there will be an area of the exterior regions which is not the simple half-space (for example, an intrusion of the upper medium into the bottom half space). In this case, one must use a larger bounding surface and introduce additional unknown point sources along the actual surface deformation. We will not consider this case in this paper.

Taking N sources with unknown amplitudes $\{a_i\}$ in the exterior region (representing the interior field) and N sources in the interior region b_i(representing the exterior field), the continuity equations across the bounding curve become, first, for the continuity of the pressure field,

$$\sum_{i=1}^{N} a_i G_m^f(\vec{X}_k; \vec{X}_i + \vec{\delta}_i) = \sum_{i=1}^{N} b_i G_m^w(\vec{X}_k; \vec{X}_i - \vec{\delta}_i) + p_m^{inc}(\vec{X}_k) \qquad (11)$$

and the normal derivative across the boundary

$$\frac{1}{\rho_{in}} \sum_{i=1}^{N} a_i \frac{\partial G_m^f(\vec{X}_k; \vec{X}_i + \vec{\delta}_i)}{\partial n} = \frac{1}{\rho_{ext(X_k)}} \left(\sum_{i=1}^{N} b_i \frac{\partial G_m^w(\vec{X}_k; \vec{X}_i - \vec{\delta}_i)}{\partial n} + \frac{\partial p_m^{inc}(\vec{X}_k)}{\partial n} \right).$$
$$(12)$$

In these equations we have indicated the discrete points along the curve C as $\vec{X}_i \equiv (r_i, z_i)$ and $\vec{X}_k \equiv (r_k, z_k)$. The source points are displaced slightly from
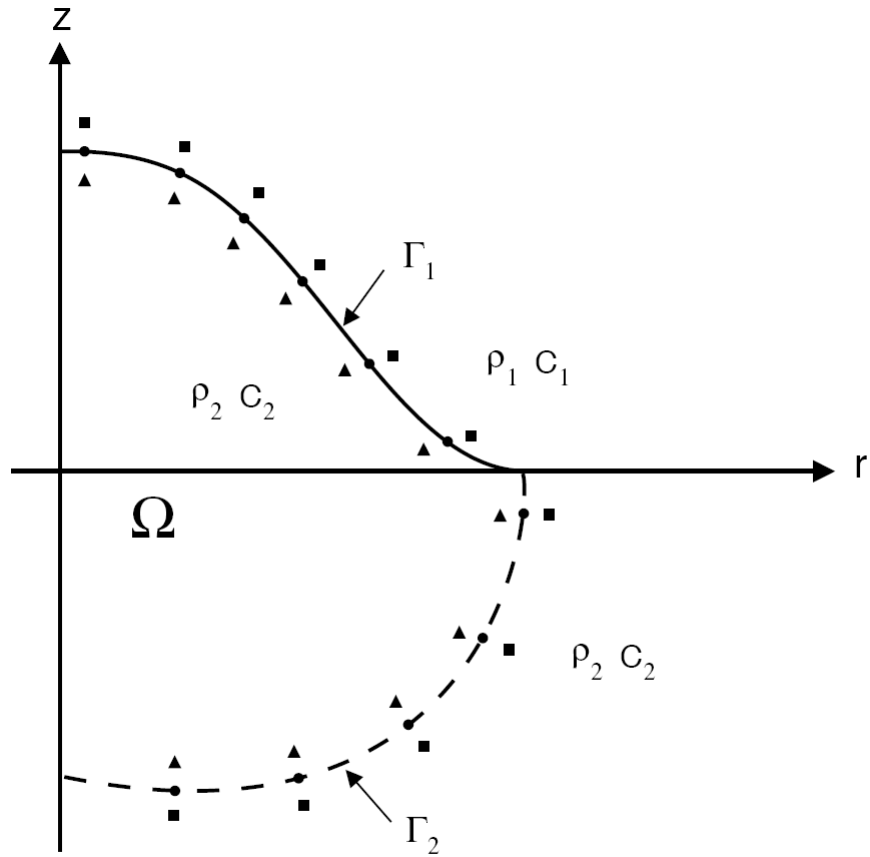
Figure 1: *A schematic of a positive bathymetric feature. The scattering chamber region Ω is surrounded by the 2 curves Γ_1 which is the surface of the feature and Γ_2 which is an additional curve introduced into the seabed to enclose Ω.*

these points, along the normal, in the positive direction $+\delta_i$ for the exterior sources and $-\delta_i$ for the interior sources. We have used the superscript f with the Green's Function in Eqs.(11) and (12) to denote free space and the superscript w to denote the surrounding waveguide. In this report we consider a 2 halfspace waveguide but the same method can also be used for the case that surrounding waveguide is bounded above by a free surface.

In the case that the bathymetric feature is a positive deformation into the water column, then $\rho_{in} = \rho_2$: for a negative deformation $\rho_{in} = \rho_1$. The density term $\rho_{ext}(\vec{X}_k)$ is equal to ρ_1 for $\vec{X}_k$ such that $z_k \geq 0$ and is equal to ρ_2 otherwise. It should also be noted that although we are stressing the modeling of scattering by three-dimensional bathymetric features, the region Ω can also model an embedded region of different sound velocity and density. In this case the interior values of c and ρ would be different from those of the 2 surrounding halfspaces.

3   A SEMI-ANALYTICAL BENCHMARK CASE

In previous references [12,13] modal solutions were derived for acoustic half-space problems in the case that the 2 halfspaces had the same sound speeds but different densities. In Ref. 13 this allowed for the solution of two-dimensional scattering from an embedded cylinder in terms of a coupled mode solution. In this paper, we will derive a corresponding three-dimensional solution. In particular, we will describe the coupled mode problem to solve for each azimuthal order m. Let us consider a sphere which is exactly half-buried between two half spaces, each with sound speed c_{ext} and densities ρ_1 and ρ_2. The sphere has an internal sound speed c_{in} and density ρ_{in}. In the case that $c_{in} = c_{ext}$ and $\rho_{in} = \rho_1$ we have a basin problem and for $\rho_{in} = \rho_2$ we have a positive deformation problem. The general solution in the interior of the sphere can be expanded in terms of the angular functions,

$$\psi_n^m(\phi, R) = N_n^m P_n^m(\cos \phi). \tag{13}$$

where P_n^m denotes a Legendre Function, and N_n^m is the normalization constant such that

$$\int_0^\pi \frac{1}{\rho_{in}} (\psi_n^m(\cos \phi))^2 \sin \phi d\phi = 1. \tag{14}$$

This angular function has the associated radial function, $j_n(k_{int}R)$ where j_n denotes a spherical Bessel Function.

In the exterior domain, the angular functions have the form for $n = 0, 2, 4, ...,$

$$\tau_n^m(\cos \phi) = P_{n+m}^m(\cos \phi) \qquad 0 \leq \phi \leq \pi \tag{15}$$

and for $n = 1, 3, 5, ...,$

$$\begin{aligned} \tau_n^m(\cos \phi) &= P_{n+m}^m(\cos \phi) & 0 \leq \phi \leq \pi/2 \\ \tau_n^m(\cos \phi) &= \frac{\rho_2}{\rho_1} P_{n+m}^m(\cos \phi) & \pi/2 \leq \phi \leq \pi. \end{aligned} \tag{16}$$

These modal functions are then normalized such that

$$\int_0^\pi \frac{1}{\rho(\phi)} (\tau_n^m)^2 (\cos \phi) \sin \phi d\phi = 1. \tag{17}$$

The associated radial functions for these angular functions are $h_n(k_{ext}R)$. The density term $\rho(\phi)$ in Eq.(17) is simply ρ_1 for $0 \leq \phi \leq \pi/2$ and ρ_2 for $\pi/2 \leq \phi \leq \pi$. The specified form of the angular modal functions is used because

for $n + m = m, m + 2, m + 4, ...$ the associated Legendre functions are even (and have zero derivative with respect to ϕ) and thus are continuous across $z = 0, \phi = \pi/2$ and trivially satisfy

$$\frac{1}{\rho_1}\frac{\partial \tau}{\partial \phi} = \frac{1}{\rho_2}\frac{\partial \tau}{\partial \phi} \quad \text{at} \qquad \phi = \pi/2. \tag{18}$$

The Legendre functions $P^m_{n+m}(\cos\phi)$ are odd with respect to ϕ at $\phi = \pi/2$ for $n = 1, 3, 5, ...$ and thus, in fact, the definition of τ as in Eq.(16) is continuous (zero) at $\phi = \pi/2$ and satisfies the boundary condition of Eq.(18). We can now set up a system of equations to be satisfied along the surface (in this coordinate system, $R = a$ and $0 \le \phi \le \pi$) of the sphere,

$$\sum_{i=0}^{N} c_i \psi_i(\cos\phi) j_{i+m}(k_{in}R) = \sum_{i=0}^{N} d_i \tau_i(\cos\phi) h_{i+m}(k_{ext}R)$$

$$+ \sum_{i=0}^{N} 2ik_ext\tau_i(\cos\phi) j_{i+m}(k_{ext}R) h_{i+m}(k_{ext}R_s)\tau_i(\cos\phi_s) \tag{19}$$

$$\frac{1}{\rho_{in}}\sum_{i=0}^{N} c_i \psi_i(\cos\phi) k_{in} j'_{i+m}(k_{in}R) = \frac{1}{\rho_{ext}(\phi)}\left(\sum_{i=0}^{N} d_i \tau_i(\cos\phi) k_{ext} h'_{i+m}(k_{ext}R)\right.$$

$$+ \left.\sum_{i=0}^{N} 2i\tau_i(\cos\phi) k_{ext}^2 j'_{i+m}(k_{ext}R) h_{i+m}(k_{ext}R_s)\tau_i(\cos\phi_s)\right). \tag{20}$$

For the system of equations in Eq.(19), we project $1/\rho_{in}\psi_j(\cos\phi)\sin\phi$, $j = 0, ..., N$ on both sides and integrate. For the systems of equations in Eq.(20) we project $\tau_j(\cos\phi)\sin\phi$ on both sides and integrate. The last terms in Eqs.(19) and (20) are the expansion of the incident field from a point source (of the form $\exp(ikR)/R$) located (in spherical coordinates) at $(R_s, \phi_s, \theta = 0)$. The resulting system of equations has the matrix/vector form

$$\begin{pmatrix} D_1 & R_1 \\ R_2 & D_2 \end{pmatrix} \begin{pmatrix} \vec{c} \\ \vec{d} \end{pmatrix} = \begin{pmatrix} \vec{r}_1 \\ \vec{r}_2 \end{pmatrix}. \tag{21}$$

Here D_1 and D_2 are diagonal matrices with entries $j_{i+m}(k_{in}R)$ and $h_{i+m}(k_{ext}R)$ respectively. The matrices R_1 and R_2 have the form

$$R_1(p,q) = h_{q+m}(k_{ext}R)\frac{1}{\rho_{in}}\int_0^\pi \psi_p(\cos\phi)\tau_q(\cos\phi)\sin\phi d\phi, \tag{22}$$

$$R_2(p,q) = j_{q+m}(k_{in}R)\frac{1}{\rho_{in}}\int_0^\pi \psi_q(\cos\phi)\tau_p(\cos\phi)\sin\phi d\phi. \tag{23}$$

The solution of the system of equations of Eq.(21) yields the interior coefficients $\vec{c}$ and the exterior coefficients $\vec{d}$ which can then be used to compute the scattered $\hat{p}_{sc}(r, z; m)$ and total pressure fields $\hat{p}(r, z; m)$. The scattered pressure field is defined as the difference between the total field and the incident field which would exist in the absence of the boundary feature. These two-dimensional fields are computed for M values of the azimuthal order m and the three-dimensional fields are then computed (for example, the scattered field) from

$$p_{sc}(r, z, \theta) = \sum_{m=0}^{M} \epsilon_m \hat{p}_{sc}(r, z; m) \cos(m\theta) \tag{24}$$

where $\epsilon_m = 1$ for $m = 0$ and $\epsilon_m = 2$ otherwise.

4 NUMERICAL COMPUTATIONS

The system of equations for the more general case of the two halfspaces having different sound velocities, Eqs.(11) and (12) is very similar to Eqs.(19) and (20) but now we use the conditions at the N values of $\vec{X}_k$ to solve for the coefficients $\{a_i\}$ and $\{b_i\}$ of the displaced point sources. Once these coefficients have been computed, they can be used in conjunction with the appropriate Green's Function to compute the scattered and total fields within the 2 halfspaces. This is done for each azimuthal order m. The final solution is computed from the azimuthal sums of the form of Eq.(1). In cases where the incident pressure field is added to the solution (for example, to compute the total field in the exterior region), the incident field is computed only once in the form,

$$p^{inc}(r, z; r_s, z_z) = \int_0^\infty J_0(p|r - r_s|)K(p; z_s)p\,dp \tag{25}$$

where $K(p; z_s)$ represents the appropriate kernel for the upper or lower half-space. In other words, we compute the incident field with a three-dimensional expression with the origin at the source position.

For the benchmark, density-jump modal case, the scattering region was a half-buried sphere. One could allow for different fractions of burial by using functions based upon a displaced centre of the sphere. However, in this case the coupling equations would be more complicated and the surface of the region would not be a constant range surface for this new centre. Thus, for the benchmark modal solution we will only consider the half-buried situation. However, the Scattering Chamber Wavefield Superposition (SCWS) approach can be used for more arbitrarily-shaped surfaces.

4.1 Density-jump benchmark solution

As a first numerical benchmark we will use both the benchmark modal approach and the SCWS approach. We will consider a spherical region (radius = 1.0 m) with an interior sound speed $c_p = 1500\ m/s$ and $\rho = 1 g/cm^3$. The upper surrounding half space has a sound speed of 1500 m/s and a density of $1\ g/cm^3$ and the lower half space a sound speed of 1500 m/s and a density of $5\ g/cm^3$. This scenario represents a half-spherical basin intruding into the lower, high-density half space. A point source is located at a range of 10 m and an angle of 5° from the z-axis. The bounding chamber is simply a half-circle in the (r, z)-space in this case. A total of 122 points were used to discretize this curve. The external and internal point sources (in the azimuthal domain) were displaced a distance of 0.05 m along the normal direction. The resulting

system of equations to solve is 244×244. The number of azimuthal terms used was given by the expression $n_m = 2\pi f/1500 \times 1.5 + 9$. As a benchmark solution we use the modal solution, using the same number of azimuthal terms as for the scattering-chamber approach. The number of modes considered for each azimuthal order is given by the expression, $n_{mode} = 2\pi f/1500 \times 3 + 16$. In Fig. 2 we show a comparison of the computed total fields along the line $z = 0$ (solid line is modal solution, dashed is scattering chamber approach). As can be seen, the agreement is excellent. The points $x = \pm 1$ are the boundaries of the basin. In Fig. 3 we show the same computations at 2500 Hz. Once again, it can be seen that the agreement with the benchmark solution is excellent. In Fig. 4 we show a grid of pressure field values computed using the scattering chamber approach. As can be seen, this "basin" has a significant effect upon the propagation and there is a strong focusing feature near the bottom. It is also important to note that there are no observable discontinuities in going across the boundary $r = 1$ where r denotes the distance from the origin. The values for $x < 0$ are computed by using $\theta = \pi$ in the azimuthal sum.

The pressure field is predicted to be somewhat ill-behaved near $x = \pm 1$ $m, z = 0$ m. This is because there is a discontinuity in the normal (r) derivative at this point because of the discontinuous boundary conditions which arise on the boundary of the scattering chamber across the boundary $z = 0$. In Fig. 5 we show the real part of the amplitudes for the exterior (the first 122 points) and interior sources (the last 122 points) for $m = 1$ and $f = 2500 Hz$. As can be seen, the solutions become larger and more erratic towards $z = 0$. However, as seen from Fig. 4 they combine to give a nicely continuous solution across the boundary $r = 1$.

For the modal method, the natural coordinate system is a spherical system and the pressure grid computations (using MATLAB) were most easily vectorizable in such a coordinate system. For the SCWS approach the best coordinate system is a (r,z) coordinate system. In this approach, the computation of the halfspace Green's Function using Eqs.(7) and (9) explicitly defined the asymptotic terms involved with the density jump. The remainder wavenumber integrals are zero in this case of only a density jump. However, in order to simplify the vectorizing of the grid computations once the coefficients have been determined, the wavenumber integral approach (for example, Eq.(7) with the determined coefficients for the external field) is used with the asymptotic and direct terms included. Some care must be taken with these integrals (in terms of the upper limit of the integral and its offset into the complex-p plane) to ensure that meaningful results are obtained for very short source/receiver ranges in the computations.

Figure 2: *A comparison of the computed pressure files for the basin scattering feature - 500 Hz, modal solution (solid line) and scattering chamber method (dashed line)*
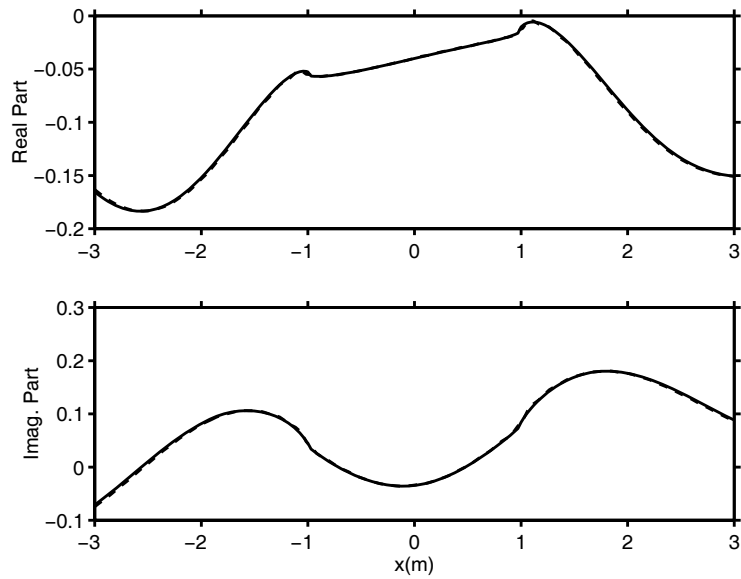

Figure 3: *A comparison of the computed pressure files for the basin scattering feature - 2500 Hz, modal solution (solid line) and scattering chamber method (dashed line)*

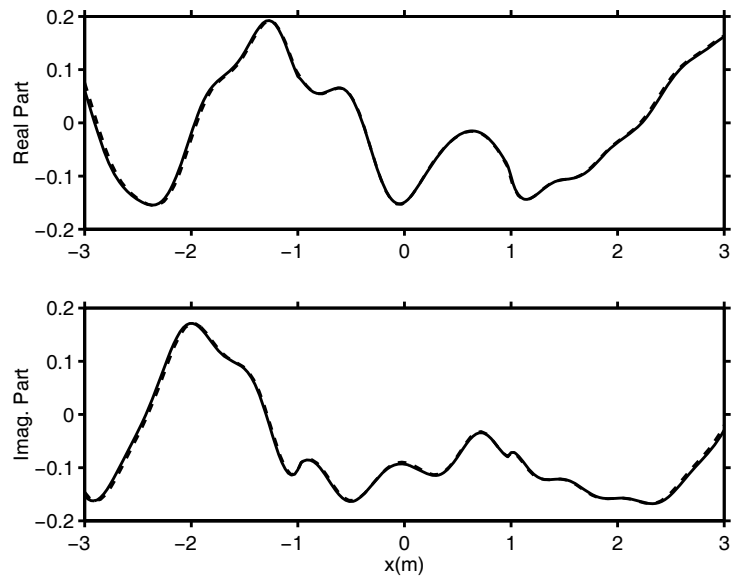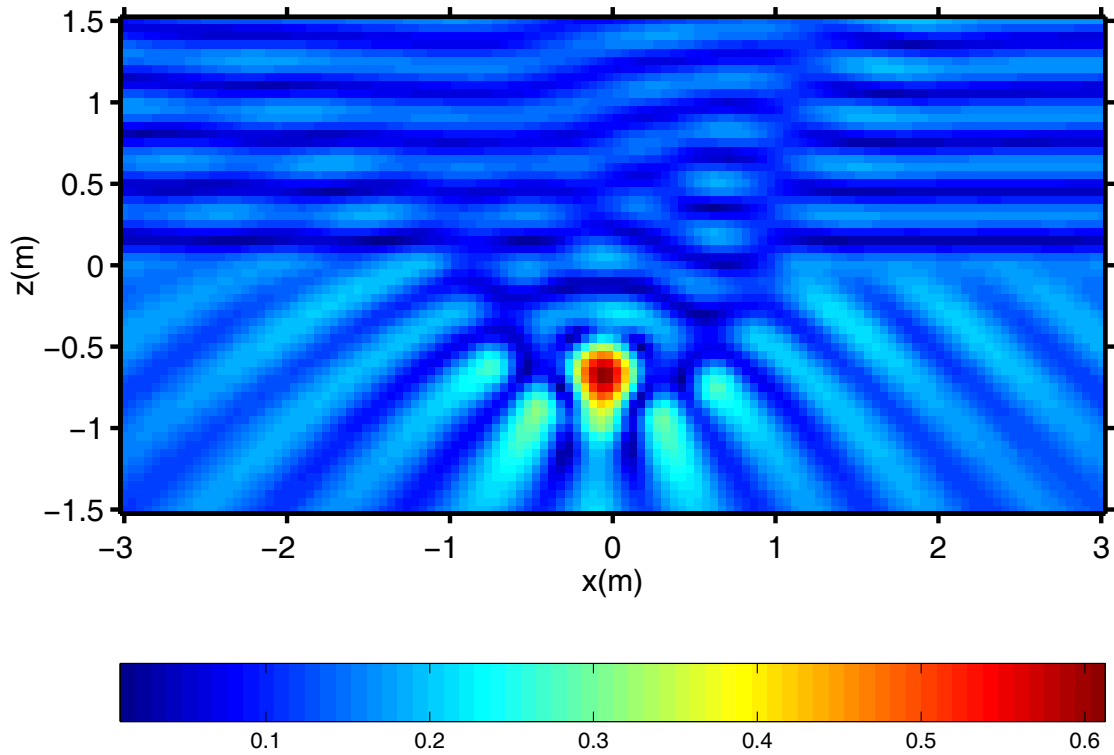**Figure 4:** *Computed two-dimensional vertical slice of the three-dimensional pressure field using the scattering chamber approach at 2500 Hz. The basin feature is evident and the incident field is due to a point source located 10 m away and at 5° off vertical*
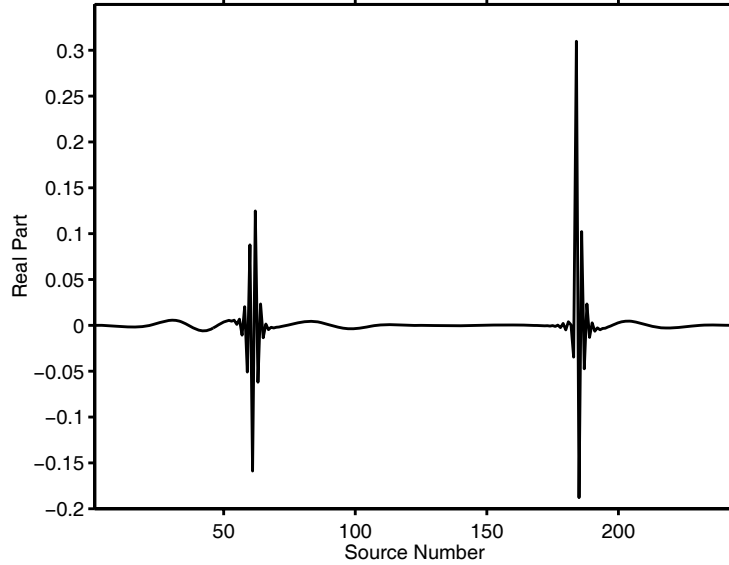
Figure 5: *The real part of the solution for $m = 1$ for the point source amplitudes for the scattering chamber approach at 2500 Hz. The values near 61 and 183 represent the solution near $r = 1$ m and $z = 0$.*

4.2 A general seabed feature

We now consider the more general situation of an axisymmetric feature with the surrounding halfspace consisting of one fluid c_1,ρ_1 overlying the seabed c_2,ρ_2. The method we propose is also easily extendable to the case of waveguide where, for example, there might be an upper bounding pressure release surface. In this case, we simply replace the half space Green's functions for the exterior region with the appropriate waveguide Green's function. We consider the following analytical expression for the deformation of the seabed,

$$z(r) = \frac{a}{2}(1 + \cos(\frac{2\pi r}{w})). \tag{26}$$

We will consider $a = 2$ and $w = 4$; this is a "bump" which has a height of 2 m and a radial extent of 2 m. It is important to recall that actual feature is this feature rotated about the z-axis, so that the true lateral extent in a horizontal slice is 4 m. A point source in the water column at 10 m range and at a height of 1 m above the seabed is considered. For the upper medium, $c_1 = 1500$ m/s, $\rho_1 = 1g/cm^3$ and for the lower sediment $c_2 = 1800$ m/s and $\rho_2 = 1.5g/cm^3$. The lower medium has an attenuation of 0.3 dB/λ. The two-dimensional slice of the scattering feature, the additional bounding curve in the bottom, and the source points are shown in Fig. 6. The number of azimuthal terms used in the computation varied with respect to frequency according to the relation $n_m = 6\pi f/1500 + 6$. This results in 37 (38, including

$m = 0$) azimuthal terms for the frequency of 2500 Hz. In the MATLAB matrix inversion we set the singular value tolerance at 10^{-8} as the system matrix tended to have conditioning issues for high azimuthal orders. As with the density contrast benchmark solutions, there are 122 interior and exterior point sources. The distance of these sources from the curve is important in obtaining accurate solutions and it was found that optimal position varied somewhat with frequency. For lower frequencies, the distance was greater than at higher frequencies. This is reasonable if one considers the longer wavelength at lower frequencies. In the following we compute the pressure fields for frequencies between 500 and 2500 Hz in steps of 25 Hz. After some numerical experimentation with these distances, we used the expression

$$d(f) = .12 - (f - 500)/750 \times .04 \qquad 500 \ Hz <= f <= 1250 \ Hz$$
$$d(f) = 0.08 \qquad 1250 \ Hz < f <= 2500 \ Hz \qquad \text{with} \qquad (27)$$
$$d(f) = 0.07 \qquad 1725 \ Hz <= f <= 1925 \ Hz, \qquad (28)$$

for our computations. This sequence of distances yielded good scattering results as a function of frequency over the band. In fact, the first two set of distances in Eq.(28) yielded sufficiently good results. However, an inspection of the computed scattered fields as a function of frequency indicated a slightly spurious response at 1725 Hz in terms of the backscattered energy. Although this anomaly is small and is insignificant in subsequent time domain computations, it is an indication that the computational parameters are not optimal in this frequency regime and we found that decreasing the distance improved the results for this frequency resulting in the point source offsets of the third case of Eq.(28). This illustrates a problem with the method for multifrequency computations. There are a number of computational parameters which need to be specified for the method: the number of discrete points, the additional contour added in either the seabed or water column, the offsets of the points sources from the curves C_1 and C_2, and even the parameters used in the numerical computation of the Green's Functions. It is desirable to have simple formulae to specify these parameters as the frequency is varied in the numerical code to automatically compute the pressure field as a function of frequency. However, the computational results did seem somewhat sensitive to the specification of the point source offsets and the parameters for the wavenumber integral for the Green's functions. Some care and numerical experimentation was required to determine good parameter values as a function of frequency.

In Figs. 7 and 8 we show the computed fields for 6 different frequencies for a vertical grid of receiver locations and for a horizontal grid at a fixed vertical distance of z = 0.55 m. In these figures there are no observable discontinuities of the field across the surface and the additional bounding curve in the bottom. It is interesting to note that since the feature is penetrable, some energy
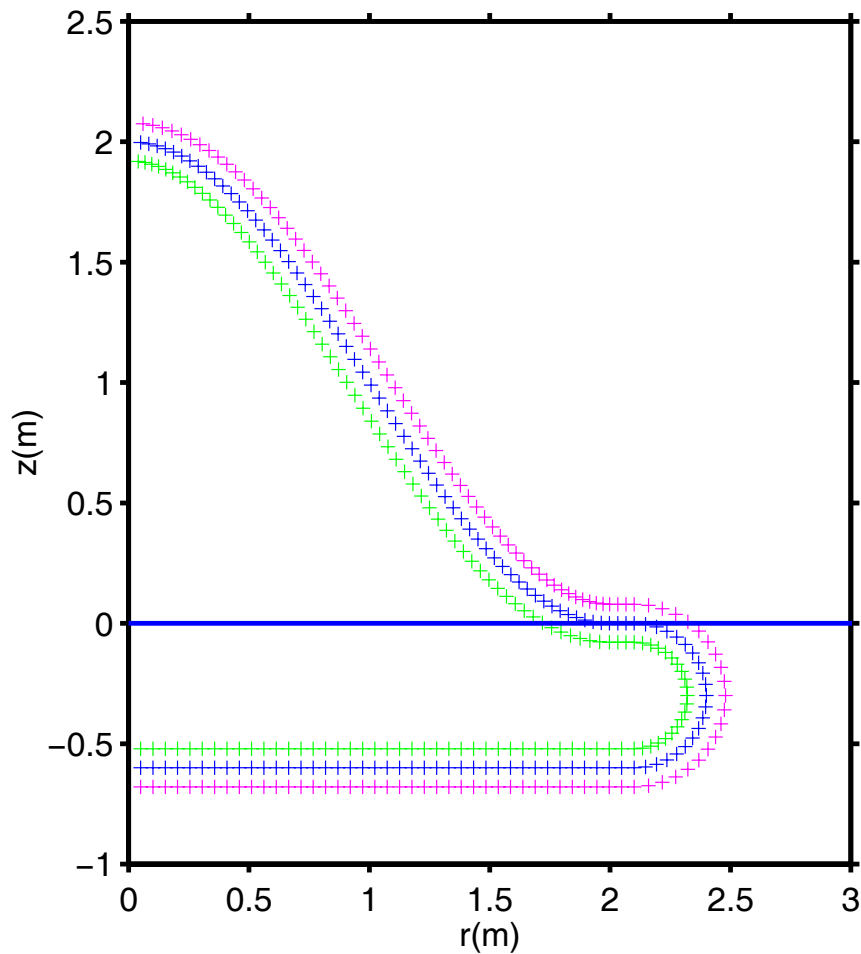
Figure 6: *Two-dimensional cross-section of bathymetric feature. The portion above $z = 0$ is the actual feature. A smooth bounding curve is added in the bottom. The blue plus signs are the discrete points along the curves where the continuity equations are imposed. The green plus signs are the source points interior to the domain which represent the scattered fields in the exterior; the half space Green's Function (in the azimuthal domain) are used for these sources. The maroon plus signs represent the fields within the domain and these use the free space Green's Function for the interior values of sound speed (complex in the case of attenuation).*
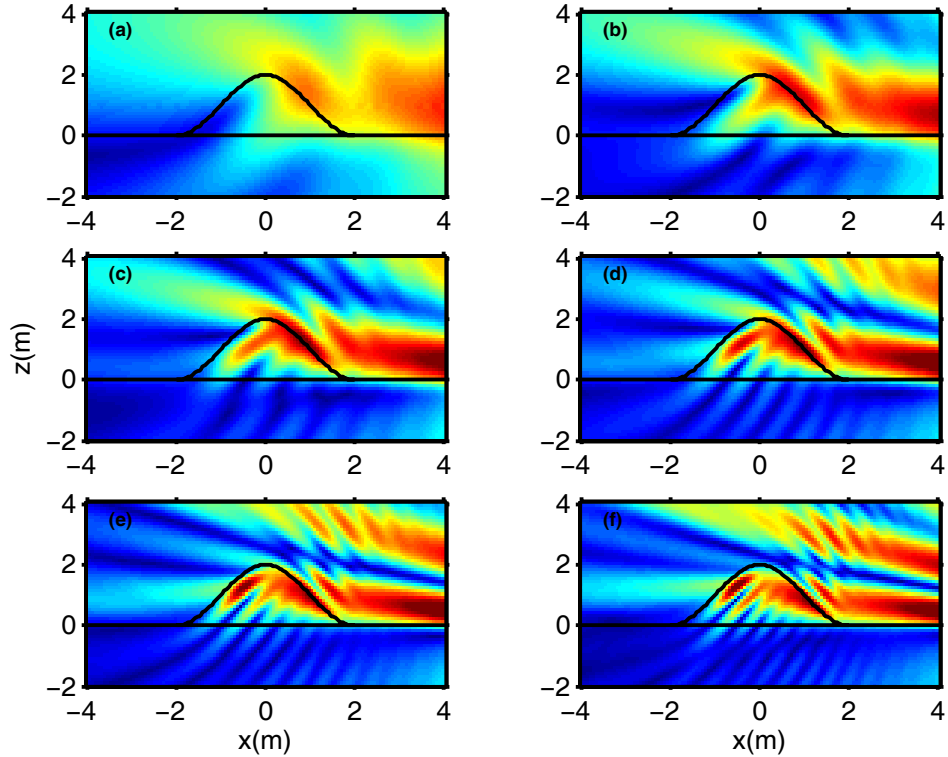
Figure 7: *Two-dimensional vertical ($y = 0$ m) cross-section of the total pressure field for 6 different frequencies: (a) 500 Hz (b) 900 Hz (c) 1300 Hz (d) 1700 Hz (e) 2100 Hz (f) 2500 Hz. The point source is to the right of the figure (off the grid). The absolute values of the levels are shown in the interval [0 0.3])*

propagates into the bump and out the other side. In Fig. 8 the circle denotes the boundary of the bathymetric feature at this altitude above the seabed and hence the acoustic parameters within this circle correspond to those of the seabed. As one would expect, the interference patterns between the direct and reflected incident fields and the scattered field become more complicated for higher frequencies.

In Fig. 9 we show the variation of the absolute value of the total and scattered fields as a function of frequency for a fixed point in the grid (x=1.23 m, z=2.05 m) which is a point of moderate scattering. As can be seen the 2 curves are well behaved as a function of frequency. We did find that the scattered field amplitudes did show more significant fluctuations as a function of frequency, particularly for the higher frequencies, at fixed grid locations close to the surface of the feature. In this case, some of these fluctuations may be due to the closeness of the receiver points to either the interior or exterior point sources combined with any numerical inaccuracies in the point source ampli-

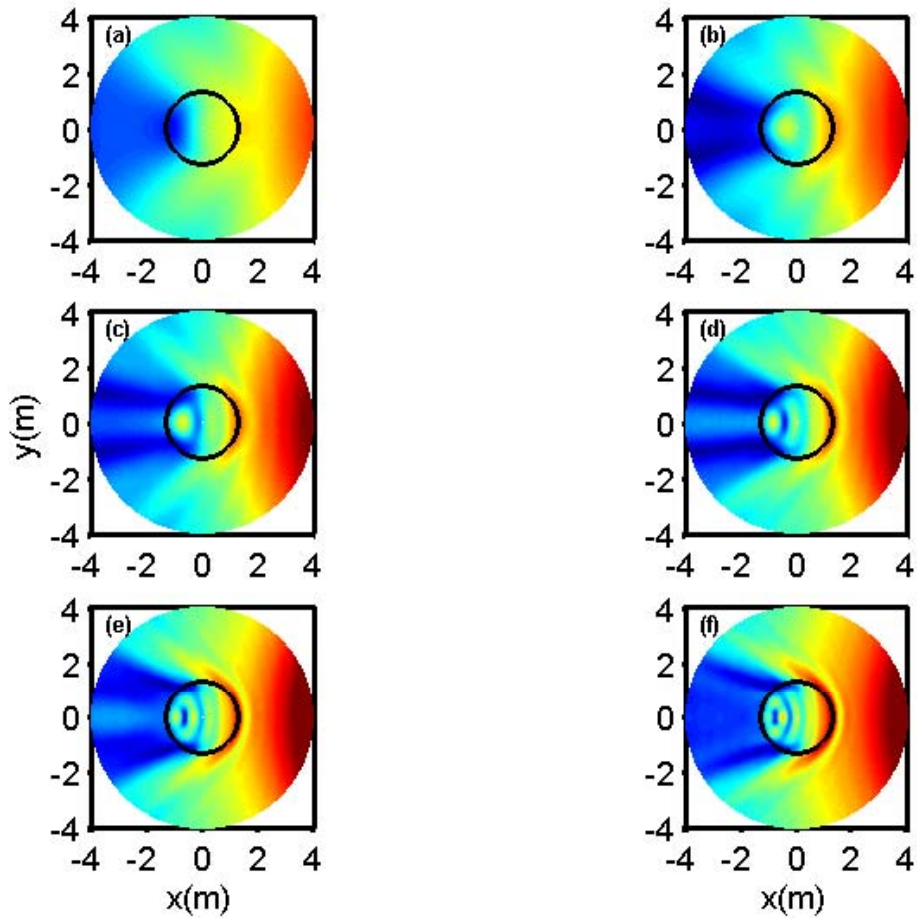**Figure 8:** *Two-dimensional horizontal cross-section (for fixed $z = 0.55\ m$) of the total pressure field for 6 different frequencies: (a) 500 Hz (b) 900 Hz (c) 1300 Hz (d) 1700 Hz (e) 2100 Hz (f) 2500 Hz. The point source is to the right of the figure (off the grid). The absolute values of the levels are shown in the interval [0 0.3]. The circle indicates the boundary of the bathymetric feature at $z = 0.55\ m$.)*
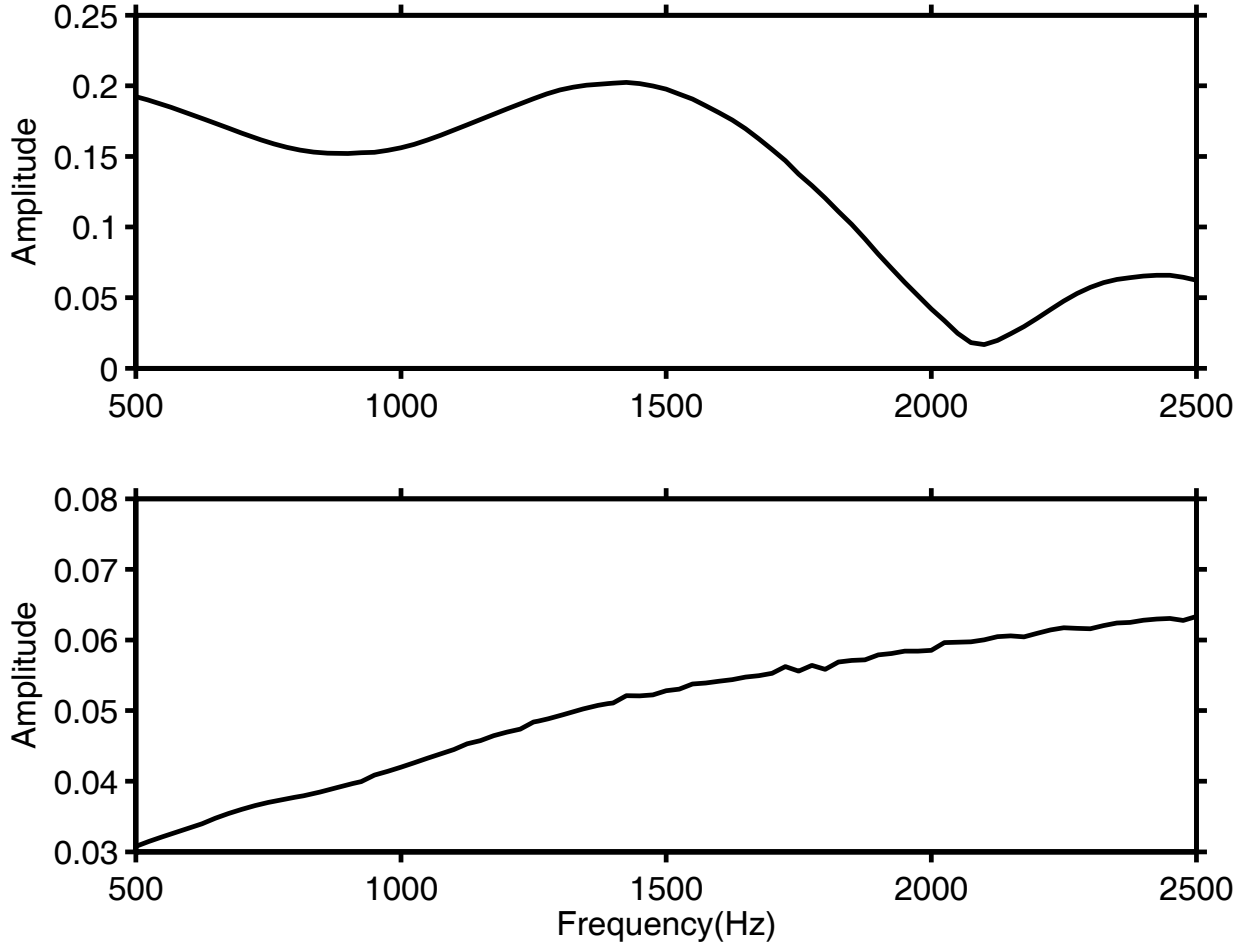
Figure 9: *The variation of the absolute value of the total field (top panel) and scattered field (bottom panel) for the point* $(x, y, z) = (1.23m, 0.0m, 2.05m)$

tudes and numerical inaccuracies in computing the resulting pressure values (particularly for locations very close to the point sources).

In Figs. 10 - 12 we show some time domain computations. The frequency results were transformed from the frequency domain to the time domain by using the expression,

$$p(x, y, z, t) = \Re\Big\{\sum_{n=1}^{N} p(x, y, z; f_n) \exp(-i2\pi f_n t) S(f_n)\Big\} \qquad (29)$$

where for the source weighting we used

$$S(f) = \exp(-(f - 1500)^2/(2 \times 500^2)). \qquad (30)$$
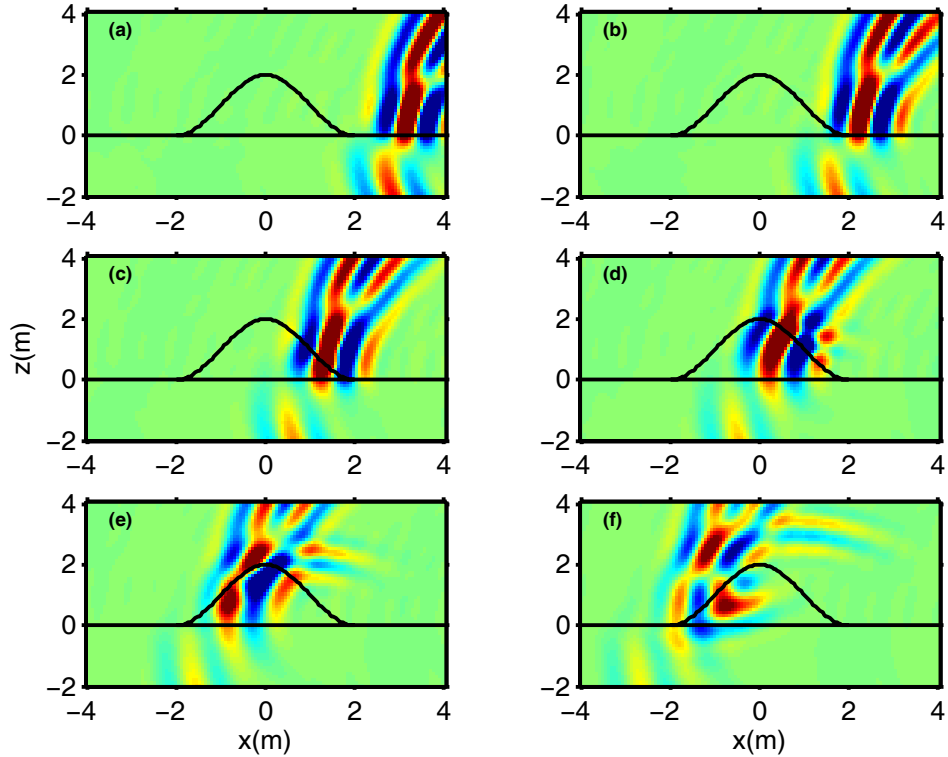
Figure 10: *Two-dimensional vertical ($y = 0$ m) cross-section of the total pressure field for 6 different times: (a) 4.5 ms (b) 5.1 ms (c) 5.7 ms (d) 6.3 ms (e) 6.9 ms (f) 7.5 ms. The point source is to the right of the figure (off the grid). The values are shown in the interval [-5. 5.])*

In Fig. 10 the resulting pulses are shown for a vertical plane for 6 instances of time. The pulse is propagating from the right to the left of the plot. The incident pulse, in the seabed, is slightly ahead of the pulse in the water because of the higher sound speed in the seabed. The pulse can be seen to travel up the scattering features and also through the feature. A reflected wavefront begins to appear in panel(d).

In Fig. 11 the propagation of the pulse in a horizontal plane can be seen. In Panel (c) the wavefront is just entering into the feature at this depth and begins to pull ahead of the wavefront on the outside. There is a significant focusing of energy within the feature. In Fig. 12 we consider this interior scattering with a finer time sampling where a reflected wavefront can be seen quite noticeably within the feature. This wavefront exits the feature into the water but is quite weak at this point.

Figure 11: *Two-dimensional horizontal ($z = 0.55\ m$) cross-section of the total pressure field for 6 different times: (a) 4.5 ms (b) 5.1 ms (c) 5.7 ms (d) 6.3 ms (e) 6.9 ms (f) 7.5 ms. The point source is to the right of the figure (off the grid). The values are shown in the interval [-5. 5.]. The circle indicates the boundary of the bathymetric feature at $z = 0.55\ m$.)*

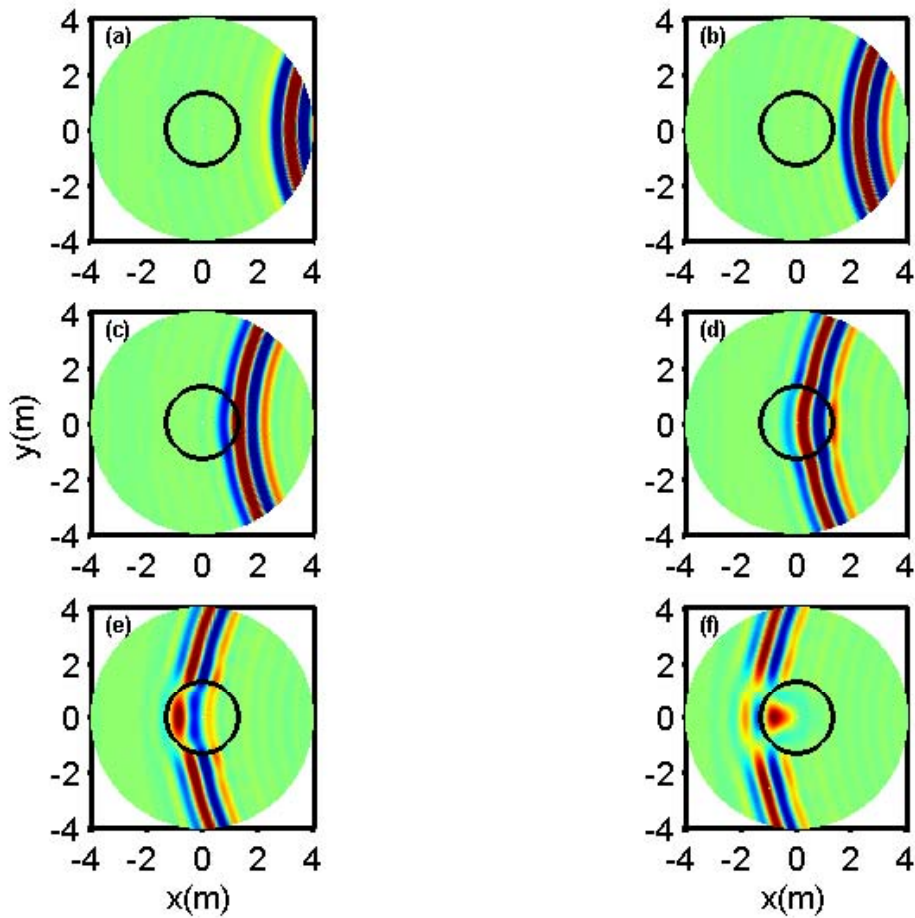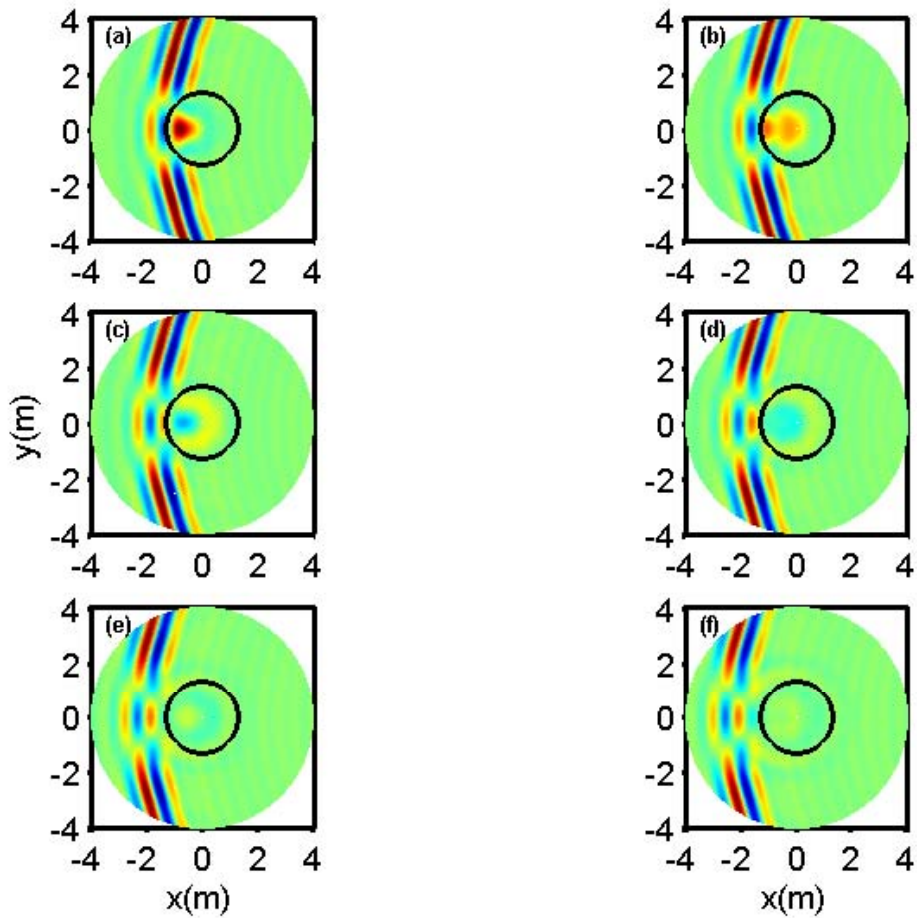**Figure 12:** *Two-dimensional horizontal ($z = 0.55\ m$) cross-section of the total pressure field for 6 different times: (a) 7.50 ms (b) 7.65 ms (c) 7.80 ms (d) 7.95 ms (e) 8.10 ms (f) 8.25 ms. The point source is to the right of the figure (off the grid). The values are shown in the interval [-5. 5.]. The circle indicates the boundary of the bathymetric feature at $z = 0.55\ m$.)*

5   SUMMARY

In this memorandum we have described an approach for computing the pressure field scattered from three-dimensional seabed features. The features were taken to be azimuthally-symmetric and the deformation to the surrounding flat seabed was taken to be of one polarity (positive - a "bump" and negative a "basin"). The computational method solved a sequence of two-dimensional problems and then used Fourier synthesis to construct the full three-dimensional solution. A benchmark coupled mode solution for the case of a hemispherical deformation with a density-contrast seabed was considered. This type of solution was used to show that the wave superposition/scattering chamber approach was very accurate for this case. This more general method was then used to solve the scattering from a 2 m high, penetrable "bump". The pressure field was accurately computed for a large range of frequencies for both vertical and horizontal planes. At the highest frequency, 37 azimuthal orders were computed. The multi-frequency computations allowed for the computation of time domain solutions for an incident pulse. Computationally, the method is straightforward. However, it was found that some care had to be taken with the positioning of the point sources.

References

1. M.D. Collins and S. Chin-Bing, "A three-dimensional parabolic equation model that includes the effects of rough boundaries", J. Acoust. Soc. Am., **87**, pp.1104-1109, 1990.

2. R.B. Evans, "Stepwise coupled mode scattering of ambient noise by a cylindrically symmetric seamount", J. Acoust. Soc. Am., **119**, pp.161–167, 2006.

3. J. Fawcett, "Coupled-mode modeling of acoustic scattering from three-dimensional, axisymmetric objects", J. Acoust. Soc. Am., **102**, pp.3387-3393 (1997).

4. M.I. Taroudakis, "A coupled-mode formulation for the solution of the Helmholtz equation in water in the presence of a conical sea-mount", J. Comput. Acoust., **4**, pp.101–121 (1996).

5. F.J Sanchez-Sesma and F. Luzon, "Seismic response of three-dimensional alluvial valleys for incident P,S, and Rayleigh waves", Bull. Seismol. Soc. Am., **85**, pp.269–284 (1995).

6. M. Imhof, "Computing the elastic scattering from inclusions using the multiple multipoles method in three dimensions", Geophysical Journal International, **156**, pp.287–296 (2004).

7. A. Sarkissian, "Multiple scattering effects when scattering from a target in a bounded medium", J. Acoust. Soc. Am.,**96**, pp.3137–3144 (1994).

8. H. Schmidt, "Virtual source approach to scattering from partially buried elastic targets", *Proceedings of High Frequency Acoustics Conference*, San Diego, March 1-5 (2004).

9. D.R. Burns, "Acoustic and elastic scattering from a seamount in three dimensions - A numerical study", **92**, pp.2784–2791 (1992).

10. J. Fawcett "A scattering-chamber approach for solving finite rough surface scattering problems", J. Acoust. Soc. Am., **118**, pp. 1348–1357 (2005).

11. J. Grannell, J Shirron and L. Couchman, "A hierarchic p-version boundary-element method for axisymmetric acoustic scattering and radiation", J. Acoust. Soc. Am., **95**, pp. 2320–2329 (1994).

12. D. Chu, "Exact solution for a density contrast shallow water wedge using normal coordinates," J. Acoust Soc. Am., **87**, pp. 2442-2450, (1990).

13. J. Fawcett, "The computation of the scattred pressure field from a cylinder embedded between two half-spaces", J. Acoust Soc. Am., **99**, pp.2435–2438 (1996).

Distribution List

Internal Distribution

David Hopkin,
Underwater Force Protection Group,
9 Grove St.,
Dartmouth, Nova Scotia, B2Y 3Z7

John Fawcett,
Underwater Force Protection Group,
9 Grove St.,
Dartmouth,Nova Scotia, B2Y 3Z7

Juri Sildam,
Torpedo Defence Group,
9 Grove St.,
Dartmouth,Nova Scotia, B2Y 3Z7

Library (5)

External Distribution

NDHQ/DRDKIM

This page intentionally left blank.

DOCUMENT CONTROL DATA			
(Security classification of title, body of abstract and indexing annotation must be entered when the overall document is classified)			

1. ORIGINATOR (the name and address of the organization preparing the document. Organizations for whom the document was prepared, e.g. Centre sponsoring a contractor's report, or tasking agency, are entered in section 8.) Defence R&D Canada - Atlantic, P.O. Box 1012, Dartmouth, N.S., B2Y 3Z7		2. SECURITY CLASSIFICATION (overall security classification of the document including special warning terms if applicable). UNCLASSIFIED	

3. TITLE (the complete document title as indicated on the title page. Its classification should be indicated by the appropriate abbreviation (S,C,R or U) in parentheses after the title). Modelling scattering from simple three-dimensional bathymetric features using wavefield superposition			

4. AUTHORS (Last name, first name, middle initial. If military, show rank, e.g. Doe, Maj. John E.) Fawcett, John A.			

5. DATE OF PUBLICATION (month and year of publication of document) August 2006	6a. NO. OF PAGES (total containing information Include Annexes, Appendices, etc). 25 (approx.)	6b. NO. OF REFS (total cited in document) 13	

7. DESCRIPTIVE NOTES (the category of the document, e.g. technical report, technical note or memorandum. If appropriate, enter the type of report, e.g. interim, progress, summary, annual or final. Give the inclusive dates when a specific reporting period is covered). Technical Memorandum	

8. SPONSORING ACTIVITY (the name of the department project office or laboratory sponsoring the research and development. Include address). Defence R&D Canada - Atlantic PO Box 1012 Dartmouth, NS, Canada B2Y 3Z7	

9a. PROJECT OR GRANT NO. (if appropriate, the applicable research and development project or grant number under which the document was written. Please specify whether project or grant). 11CL	9b. CONTRACT NO. (if appropriate, the applicable number under which the document was written).

10a ORIGINATOR'S DOCUMENT NUMBER (the official document number by which the document is identified by the originating activity. This number must be unique to this document.) DRDC Atlantic TM 2006-086	10b OTHER DOCUMENT NOs. (Any other numbers which may be assigned this document either by the originator or by the sponsor.)

11. DOCUMENT AVAILABILITY (any limitations on further dissemination of the document, other than those imposed by security classification) (X) Unlimited distribution ( ) Defence departments and defence contractors; further distribution only as approved ( ) Defence departments and Canadian defence contractors; further distribution only as approved ( ) Government departments and agencies; further distribution only as approved ( ) Defence departments; further distribution only as approved ( ) Other (please specify)

12. DOCUMENT ANNOUNCEMENT (any limitation to the bibliographic announcement of this document. This will normally correspond to the Document Availability (11). However, where further distribution (beyond the audience specified in (11) is possible, a wider announcement audience may be selected).

13. ABSTRACT (a brief and factual summary of the document. It may also appear elsewhere in the body of the document itself. It is highly desirable that the abstract of classified documents be unclassified. Each paragraph of the abstract shall begin with an indication of the security classification of the information in the paragraph (unless the document itself is unclassified) represented as (S), (C), (R), or (U). It is not necessary to include here abstracts in both official languages unless the text is bilingual).

In this report a method for modelling the scattering from three-dimensional bathymetric features on the seabed is described. In particular, the features are taken to be azimuthally symmetric about the z-axis. This approach could model seamount or basin type features or at higher frequencies, smaller protuberances and depressions. The method uses a set of point sources within the scattering region and exterior to the region to satisfy the appropriate continuity and boundary conditions along scattering features and seabed/water interface. Multi-frequency and Fourier-synthesized time domain responses for the scattering from such features are presented. In addition we present a semi-analytic modal solution which can be used as a benchmark for a bathymetric feature in a halfspace with only a change in density.

14. KEYWORDS, DESCRIPTORS or IDENTIFIERS (technically meaningful terms or short phrases that characterize a document and could be helpful in cataloguing the document. They should be selected so that no security classification is required. Identifiers, such as equipment model designation, trade name, military project code name, geographic location may also be included. If possible keywords should be selected from a published thesaurus. e.g. Thesaurus of Engineering and Scientific Terms (TEST) and that thesaurus-identified. If it not possible to select indexing terms which are Unclassified, the classification of each should be indicated as with the title).

three-dimensional, scattering, superposition

This page intentionally left blank.

Defence R&D Canada

Canada's leader in defence
and National Security
Science and Technology

R & D pour la défense Canada

Chef de file au Canada en matière
de science et de technologie pour
la défense et la sécurité nationale

DEFENCE R&D DÉFENSE

www.drdc-rddc.gc.ca